Joint sensing and communication: Coverage analysis of downlink based on stochastic geometry

Abstract

aaaaaaaaaaaaa aaaaaaaaaa aaaaaaa aaaaaaaaaaaa aaaaaa aaaaaaaa aaaaaaaa aaaaaaaa aaaaaaaaaaaaaa aaaaaaaaaaaa aaaaaaaaaa aaaaaaaaaaaaaaa

Index Terms

Joint sensing and communication, Stochastic geometry, Coverage probability, Power allocation, Spectrum allocation.

I. Introduction

Current communications and perception applications tend to be independent, such as 5G communication and GPS. They are designed in different systems, and even at some stages, they share the same devices and similar technologies. One of the hot topics in the 6G era is that communication and perception will be integrated and regarded as joint sensing and communication, where features of sensing and communication will be joint considered and fused to enhance both sensing and communication functions.

In [1],

In the current communication scenario, due to the lack of surrounding environmental (SE) and end-user position (EUP) information, we can only analyze the relevant communication theory from a statistical point of view, such as coverage probability and throughput capacity, etc.

A normal assumption is that EUP should be subject to a Poisson point process (PPP) where the positions of EUs are random. So, most of the time, due to the unknown of the EU's position, when we calculate the coverage probability and throughput, broadcast communication is considered, and no antenna gain is considered.

As the concept of joint sensing and communication (JSAC) is proposed in the 6G era, in the process of theoretical correlation analysis, the impact of the randomness of EUP will fade.

On the contrary, the gains brought by the certainty of EUP will be continuously magnified. A normal application scenario for JASC is shown in Fig. **??**.

In Fig. **??**, there are some fixed targets, like base stations (BS), buildings, trees, traffic lights, street lights, and so on; some moving targets, like cars, cyclists, walking people, and so on. In the current communication system, the BS needs to broadcast the paging signal to find the end-user (EU), for example, a walking man. Equipped with a sensing function, the BS can recognize the surrounding environment and send the signal to the EU directly with a beamforming gain. Another way to achieve the gain of JSAC is at the side of the end-vehicle (EV), for example, a car. Suppose the local IoT around the BS is built in the environment. In that case, when the EV gets into the local IoT, the network can update the environment status of the EV to help it become driverless or avoid danger; on the other side, the EV can also sense and update the real-time environment to the BS.

In a word, sensing can help EU or EV know the surrounding environment and help communicate with others.

==========

Matching the communication coverage radius (given a constraint of the minimum coverage probability) and the sensing radius, the ratio of communication bandwidth and sensing bandwidth is optimized to maximize the performance of the joint sensing and communication (JSAC) system.

In the joint system, a standard for the perfect collaboration between sensing and communication functions is proposed, that is, the independent maximization of a specific function should not be pursued alone, and the performance optimization of two subsystems should be considered under a dual and matched constraint, like sensing range, communication radius (with a required minimum coverage probability).

From the perspectives of the maximum sensing distance and the maximum communication rate, analyze the influence of two basic frequency division strategies (continuous frequency division and interval frequency division) on the JSAC system in the case of the sensing and communication systems working independently.

Joint optimization is analyzed to prove the superiority of the communication system under the blessing of the sensing function. Beamforming technology is applied to improve the data rate, where the location of the receiver is known.

Optimize the spectrum ratio of sensing and communication, and give insights into different

situations: when should the sensing resolution performance be emphasized and when should the communication rate performance be emphasized.

==========

A. *Related work*

Literature focusing on the coverage probability of joint sensing and communication based on stochastic geometry is revealed as follows. In [2]–[5], all the base stations, user equipment, sensing targets, radars, transmitters, and receivers are subject to independent Poison Point process (PPP).

In [2], a novel mathematical framework is proposed to characterize the joint sensing and communication (JSAC) coverage probability and ergodic capacity. In the framework where base stations (BSs), user equipment (UEs), and sensing targets (STs) are involved. An information-theoretic formulation of radar tracking is employed, and a shared multicarrier waveform and analog beamforming are used to analyze the downlink sensing and communication coverage and capacity.

BSs are responsible for the transmission of downlink communication data to UEs, the reception of uplink communication data from UEs, and the transmission of sensing waveforms used to monitor STs. UEs are responsible for the transmission of uplink communication data to BSs and the reception of downlink communication data from BSs. They may also participate in sensing STs in the network. To distinguish BS sensing from UE sensing, we shall refer to the transmission of radar waveforms by the base station as downlink sensing, and the transmission of radar waveforms by the UEs as uplink sensing following.

In [3], BSs, UEs, radars, and targets are involved in constructing JSAC, and a single transmit signal by the BS serves both sensing and communication. A downlink communication is established between BS and UE. A monostatic target-sensing link is built between the radar and the target. A bistatic target-sensing process is characterized where a straight signal transmitted by BS is received by the radar, and an echo signal (which is transmitted by the BS) reflected by the target is received by the radar. Fusion analysis of the straight signal and the echo signal is achieved at the side of the radar in order to localize the target.

In [4], effects over the network throughput made by time trade-off are analyzed in JASC. Parameters involved in radar sensing using pulse signals, such as the exploitation duty cycle, the radar bandwidth, the transmit power, and the pulse repetition interval, are considered. A bistatic

sensing model is considered in [4], where the BS transmits the sensing or communication signal with a time division schedule. The mobile user (sensing target) will reflect the sensing signal to the receiver, which is also the receiver of communication.

In [5], multi-radar cooperative detection is proposed to expand the detection region, at the same time, communication links between radars are established. In the application scenario, all the radars are divided into different tiers, in each tier, one of the radars will be selected as the fusion center. Other radars in the same tier will detect the target, collect the information about the target and then transmit the gathered information to the fusion center. Power allocation for radar detection and communication is considered. The cooperative detection region of multi-radar is analyzed since there will be some overlap detection region for different radars.

In [6], the average cooperative detection range in the application scenarios of JSAC is analyzed. Different numbers of vehicles with sensing and communication devices are placed randomly. The sensing range and communication range are given. Hence, the average overlaps of the sensing region and communication region can be calculated in different scenarios, such as two vehicles, three vehicles, and more.

In [7], pulse radars (nodes) are used in a network for target detection and data exchange. The two functions share the same wireless channel. Based on stochastic geometry tools, radar detection range and network throughput are studied. Particularly, the time-division method is applied. Nodes share a common bandwidth, and each of them operates in turn in radar mode (detect targets) and in communication mode (data exchange). The timeline is slotted, and nodes access the shared channel following a slotted ALOHA policy.

In [8], an automotive scenario including a two-lane road with vehicles and smart traffic lights is considered. All the vehicles and traffic lights are equipped with a dual-function radar and communication system. Multiple metrics are considered to evaluate the performance of JSAC, such as communication coverage probability, radar false alarm probability, radar detection probability, radar success probability, joint radar detection and communication coverage probability, and joint radar success and communication coverage probability.

In the scenario of JSAC, we can imagine that if the coverage of sensing is bigger than the communication range, the target sensing outside the communication range will appear insignificant where communication can not be built. On the other side, if the communication range is bigger than the sensing range, the communication link out of the sensing coverage area can not apply the beamforming technology since the target position can not be achieved. In this way,

broadcast communication is required and which will waste a lot of energy.

B. Contributions

- We propose that in the downlink of JSAC, the matching of ranges of sensing and communication should be regarded as a basic principles
- We propose to take joint consideration of the bandwidth and energy in JSAC. Coverage matching should be achieved between target sensing and communication, where beamforming technology can be used in communication to improve energy efficiency.
- A maximum distance resolution in target sensing and a minimum data rate are proposed as the conditions to optimize the joint coverage performance in JSAC. Besides that, the sensing-only target and the sensing-communication target are distinguished, and different target densities are used to represent different application scenarios. Tools from stochastic geometry are applied to model the system in a statistical way.
- The joint coverage performance of sensing and communication based on the joint allocation of energy and bandwidth is analyzed. Simulation results show the correctness and reliability of the mathematical analysis.
-

II. Background

A. Distance resolution in target sensing

A normal Frequency-Modulated Continuous-Wave (FMCW, which is also named a chirp signal) transmitted by a base station is shown in Fig. 1 (the blue line), where the start frequency is f_0, the bandwidth is B_s, the chirp time is T_c, so the slop of the spectrum is $S = \frac{B_s}{T_c}$. When the chirp signal from the transmitter touches some targets, the reflected signal will be back to the transmitter (base station, BS), for example, the red line, the green line, and the manganese line. t_1, t_2, and t_i mean the different time relays created by the distance between the BS and different targets. Based on Fig. 1, we can know that multiple targets can be sensed by BS easily, and the distance resolution can be derived as follows.

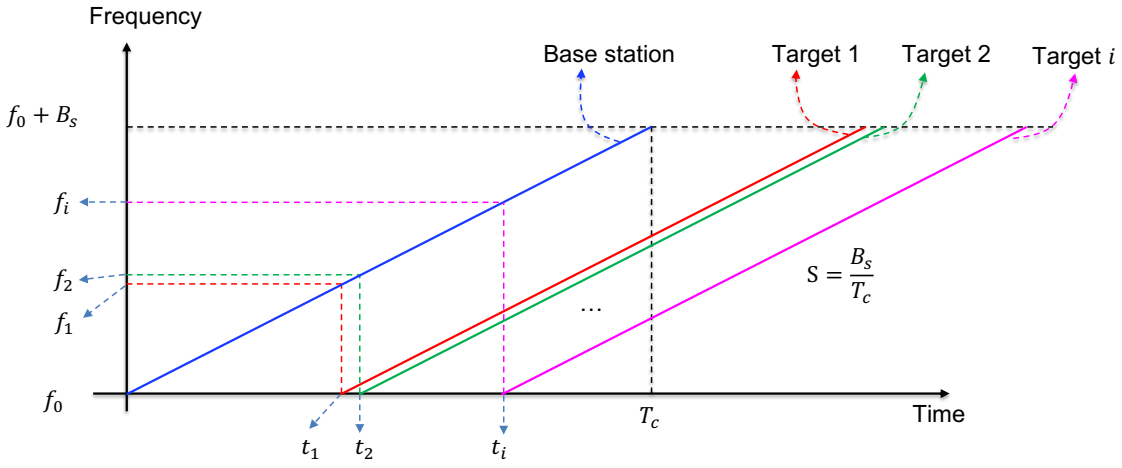

Fig. 1: A normal Frequency-Modulated Continuous-Wave

For the transmitted signal, we can model it as follows:

$$x_{\mathrm{BS}} = \sin\left(2\pi(f_0 + St)t + \phi_0\right), \quad 0 \le t \le T_c. \tag{1}$$

For the echo signal from target 1, we can model it as follows:

$$x_{\mathrm{T_1}} = \sin\left(2\pi(f_1 + St)t + \phi_1\right), \quad t_1 \le t \le t_1 + T_c. \tag{2}$$

At the same time as transmitting the sensing signal by BS, the transmitted signal will be sent to the mixer. When the BS receives the echo signal from target 1, the received signal will also be sent to the mixer, and then we can get the intermediate frequency (IF) signal as follows:

$$x_{\mathrm{IF}} = \sin\left(2\pi(|f_0 - f_1|)t + (\phi_0 - \phi_1)\right), \quad t_1 \le t \le T_c. \tag{3}$$

Hence, the frequency of the IF signal, $|f_0 - f_1| = S \times t_1$, is a constant related to the time delay (i.e., the distance between BS and target 1). Hence the distance between the BS and the target can be calculated, $d_1 = \frac{c \times t_1}{2}$. If the receiver antenna is an array, the location of the target can be calculated.

Regarding the scenario of multi-targets, distance resolution must be considered, which means the minimum distance difference between two targets that make the distinction between the two targets possible. We can assume that target 2 is a litter further away from BS than target 1. In reference to the IF signal frequency in (3), the difference in frequency between the IF signals of target 1 and target 2 is $|f_1 - f_2|$. Let $\Delta f = |f_1 - f_2|$ and we can have

$$\Delta f = S \times \Delta t = S \times \frac{2\Delta d}{c}, \tag{4}$$

where S is the slope of the spectrum, $c = 3 \times 10^8$ m/s, Δd is the distance between target 1 and target 2. Since the time difference includes the forward time and backward time, $2\Delta d$ is considered. Recall the theory of Fourier transforms. If we want to distinguish two sinusoidal signals with different frequencies, there will be a minimum observation time. Hence, we have

$$\frac{S2\Delta d}{c} > \frac{1}{T_c - t_1} \Rightarrow \Delta d > \frac{c}{2S(T_c - t_1)} = \frac{cT_c}{2B(T_c - t_1)} = \frac{cT_c}{2B_s(T_c - \frac{2d_1}{c})}, \tag{5}$$

where d_1 is the distance between BS and target 1. Hence we can have the distance resolution in sensing at a distance d away from the BS as:

$$d_{s,res}(d) = \frac{cT_c}{2B_s(T_c - \frac{2d}{c})}. \tag{6}$$

B. Channel model for target sensing

As shown in [9], the radar equation can be writeen as

$$P_{s,r}(D) = \frac{P_{s,t}g_{s,t}}{4\pi D^2} \times \frac{\rho}{4\pi D^2} \times A_e, \tag{7}$$

where $P_{s,t}$ is the transmit power for target sensing, $g_{s,t} = 10^{0.1G_{s,t}}$ where $G_{s,t}$ is the gain of the transmit antenna with the unit of dB, ρ is the radar cross-section, D is the sensing distance between the radar and the target, A_e is the receiving antenna of the effective area that collects a portion of the echo power returned to the radar. According to the antenna theory [**?**], there is a relation between the gain $g_{s,r}$ of the antenna on receive and its effective area A_e on receive, which is

$$g_{s,r} = \frac{4\pi A_e}{\lambda^2}. \tag{8}$$

where $g_{s,r} = 10^{0.1G_{s,r}}$ where $G_{s,r}$ is the gain of the receive antenna with the unit of dB, λ is the wavelength of the sensing signal.

Hence, based on the characteristics of FMCW [**?**], we can have the sensing model as

$$P_{s,r}(D) = \frac{P_{s,t}g_{s,t}}{4\pi D^2} \times \frac{\rho}{4\pi D^2} \times \frac{g_{s,r}\lambda^2}{4\pi} \times NT_c, \tag{9}$$

where N is the amount of the chirp in a frame of the sensing signal, T_c is the duration time of the chirp signal (as shown in Fig. 1).

The thermal noise power at the receiver antenna can be written as

$$n_s = KT_0B_sF_n, \tag{10}$$

where $K = 1.380649 \times 10^{-23}$ is the Boltzmann's constant with the unite of $\mathrm{m^2{\cdot}kg{\cdot}s^{-2}{\cdot}K^{-1}}$, T_0 is the standard temperature of 290 K, B_s is the bandwidth for sensing, and F_n is the noise figure of the receiver antenna.

C. Channel model for communication

Since the high frequency is used for communication signals in JSAC, the communication range will be very short compared with other normal radiocommunications. Hence, the normal free space wireless communication channel model is inapplicable. Another channel model that can be used for short-range outdoor radiocommunication system is proposed by International Telecommunication Union (ITU). Recommended by [10]–[12], the transmission loss for the millimeter-wave propagation at frequencies above 10 GHz in the outdoor short-range field ($<$ 1km) can be written as:

$$L_{LoS} = 20\log f - 28 + 19\log R + L_{gas} + L_{rain}\ \mathrm{dB}, \tag{11}$$

where f is in MHz, R is the propagation distance, L_{gas} and L_{rain} are attenuation by gases and by rain. According to [11], [12], L_{gas} and L_{rain} are independent of the propagation distance and only related to the signal frequency. Hence, For simplicity, without any influence on the analysis results, we can set L_{gas} and L_{rain} as the atmospheric absorption with a given value which is widely used [13]–[15]. In this paper, we assume $L_{gas} + L_{rain} = 2$ dB. Besides that, in mmWave communication with a frequency of around 70 GHz, additional loss and implementation loss should be considered [16], which will be indicated as L_{add} and L_{imp} in dB. For simplification

without any effect on the analysis result, L_{sum} is denoted as the summation of L_{gas}, L_{rain}, L_{add}, and L_{imp}.

Hence, we can have the channel model for the communication in JSAC as

$$P_{c,r}(R) = \frac{P_{c,t} \times 10^{2.8}}{f^2 R^{1.9} \times 10^{0.1 L_{sum}}} \tag{12}$$

III. System Model

For better traceability, distance in the communication link is indicated with a symbol of R, and distance in the sensing link is indicated with a symbol of D.

A. Structure of the joint system

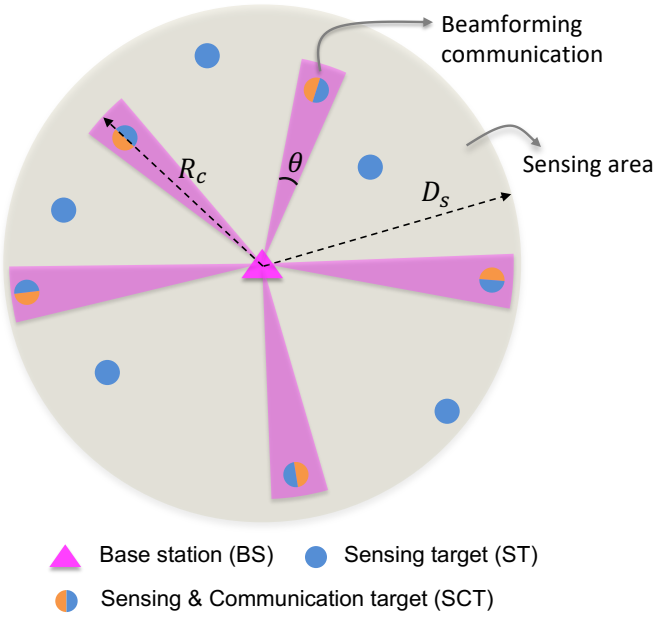

Fig. 2: System model for downlink in JSAC

A system model for downlink in JSAC is shown in Fig. 2, where base stations (BSs), sensing targets (STs), and sensing-and-communication targets (SCTs) are involved. D_s means the sensing range of the BS, R_c means the communication range between the SCT and the BS. Another pair of parameters considered in JSAC is the distance resolution in sensing and the data rate in communication, which are indicated as $D_{s,res}$ and $R_{c,com}$. In this paper, we propose to analyze

the joint coverage probability considering a restriction of a given maximum resolution $d'_{s,res}$ in sensing. Hence, we can have

$$\mathbb{P}_{\text{j,cov}} = \mathbb{P}\left[\texttt{SCNR}_s \geq \tau_s, D_{s,res} \leq d'_{s,res}, \texttt{SINR}_c \geq \tau_c\right] \tag{13}$$

where $\texttt{SINR}_c$ is the signal-to-interference and noise ratio in communication, τ_c is the threshold for decoding in communication which is achieved by the required minimum data rate $r_{c,com}$, $\texttt{SCNR}_s$ is signal-to-clutter and noise ratio in sensing, τ_s is the threshold for target detection in sensing, $d'_{s,res}$ are the given maximum distance resolution for sensing.

Regarding the random locations of BSs, STs, and SCTs in the scenario of JSAC, All of them are subject to independent homogeneous Poisson Point Processes (PPPs). STs and SCTs are distinguished and noted with different densities, γ_{st}, γ_{sct}. The density of the BSs is γ_{bs}.

Considering the downlink in JSAC, the BS can transmit signals of sensing and communication to the targets around it. In terms of sensing, BS can broadcast the sensing signal (FMCW signal) and receive the echo from the targets, and then it can obtain the locations of surrounding targets, which are noted as sensing targets.

It should be marked that with the increase of the sensing distance, the distance resolution, $d_{s,res}$, decreases. The coverage performance of sensing and distance resolution is related to the allocated transmit power and the allocated bandwidth.

In terms of downlink communication, BS can transmit data to the surrounding STs. In this way, the STs communicating with the BS are noted as sensing-and-communication targets (SCTs). Since the locations of SCTs are achieved by BS via sensing, beamforming technology can be used by downlink communication where the beam width is indicated as θ. The communication between BS and the SCT is shown in Fig. 3. To ensure that the SCT will be covered by the BS with high energy efficiency, the beamwidth θ is decided by the distance between the SCT and BS, $R_{b,t}$. We assume that all the targets will be covered by a cover diameter C_d, which is given and big enought to cover all the targets (all the BSs share with the same cover diameter). Hence, we can have the relationship between θ, $R_{b,t}$, and C_d as:

$$C_d = 2R_{b,t}\tan(\frac{\theta}{2}) \;\Rightarrow\; \theta = 2\arctan(\frac{C_d}{2R_{b,t}}). \tag{14}$$

Regarding the interfering model in sensing and communication. The PPPs of BS and Targets (including STs and SCTs) are independent. In the downlink sensing and communication, each target will be detected and communicated by the nearest BS. So, each BS and its contracted targets are indicated as a tie, and the BS is marked as tagged BS. Hence the other BSs out of

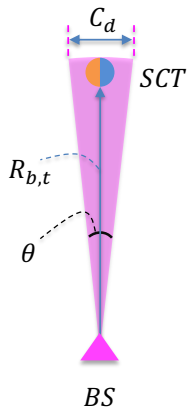

Fig. 3: Beamwidth and cover diameter of the BS

the tier are regarded as interfering BSs in the scenario of sensing and communication.

B. Interference in the downlink sensing

Considering the interference in downlink sensing, which can be shown in Fig. 4. On the side of a BS (BS in Fig. 4), which is detecting a tagged ST (ST in Fig. 4), the interference signal can be classified into three parts:

1) the interference signal comes from other BSs in other ties (BS_j in Fig. 4), which can be divided into two parts, direct-path breakthrough signal and import-clutter signal;

2) the interference signal made by other STs ($ST_i, i = 1, 2, 3, \cdots$, in Fig. 4) in the same tier with ST, which comes from the BS, arrive at ST_i, and then reflected again by ST_i to the BS, which can be named as the self-clutter signal;

3) clutter signals made by the reflection of the surrounding environment, like ground, atmospheric gases, rain, etc.

According to the IEEE standards for radar [17], the direct-path breakthrough signal can be filtered by a clutter filter group or filter bank based on the different Doppler shift. So, we can ignore the effects made by the direct-path breakthrough signal.

Regarding the difference in the Doppler shifts between the desired signal and the self-clutter signal. Since the moving directions of ST_i and ST are independent random, we can not distinguish the final Doppler shifts in the self-clutter signal and the desired signal. Hence, the self-clutter can not be rejected by the clutter filters, and it will be considered in the analysis.

Particularly, in a small range with high densities of BSs and targets, the strength of the clutter caused by the surrounding environment (the third kind of interference) is small compared with the other two kinds of interference.

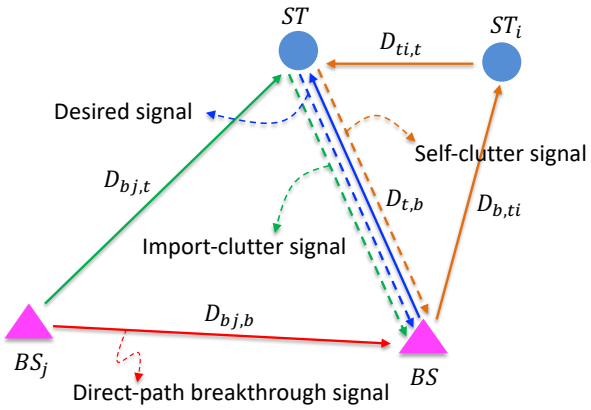

Fig. 4: Interfering model for downlink sensing in JSAC

In this paper, we focused on the first two interference and assumed the third one as a given value in dB. Besides that, thermal noise will be considered.

Distances between the BS and each interference resource are shown in Fig. 4. Based on the sensing model in (9), we can have interference in the sensing link as

$$\begin{aligned} C_s = & \sum_{j=1,2,\cdots} \left(\frac{P_{s,t} g_{s,t}}{4\pi D_{bj,t}^2} \times \frac{\rho_{st}}{4\pi D_{t,b}^2} \times \frac{g_{s,r}\lambda^2}{4\pi} \times N T_c H_{s,j} \right) \\ & + \sum_{i=1,2,\cdots} \left(\frac{P_{s,t} g_{s,t}}{4\pi D_{b,ti}^2} \times \frac{\rho_{st,i}}{4\pi D_{ti,t}^2} \times \frac{\rho_{st}}{4\pi D_{t,b}^2} \times \frac{g_{s,r}\lambda^2}{4\pi} \times N T_c H_{s,i} \right) \\ & \triangleq C_{s,1} + C_{s,2}, \end{aligned} \tag{15}$$

where $C_{s,1}$ indicates the interference caused by the import-clutter signal, and $C_{s,2}$ indicates the interference caused by the self-clutter signal.

C. Interference in the downlink communication

Considering the interference in downlink communication, code division, time division, or OFDM technology can be used in downlink communication. Hence, there is no interference between different downlinks related to different SCTs that are connected to the same tagged BS (in the same tier). On the side of SCTs, the interference comes from BSs in other tiers, and we can know that all the interfering BSs are further than the tagged BS to the SCT.

The interfering model in downlink communication is shown in Fig. 5, BS is communicating with its desired target SCT, and $BS_j, j = 1, 2, 3, \cdots$ is communicating with its desired target $SCT_j, j = 1, 2, 3, \cdots$. All the BSs has its own beamwidth, indicated as θ or θ_j, based on their desired communication distance $R_{b,t}$ or $R_{bj,tj}$. Since all the targets will build communication links with the nearest BS, we have $R_{b,t} < R_{bj,t}$, where $R_{bj,t}$ is the distance between SCT and

the interfering BS, BS_j. Based on (14), we can have the expression of the beamwidth of BS_j as:

$$\theta_j = 2\arctan(\frac{C_d}{2R_{bj,tj}}). \tag{16}$$

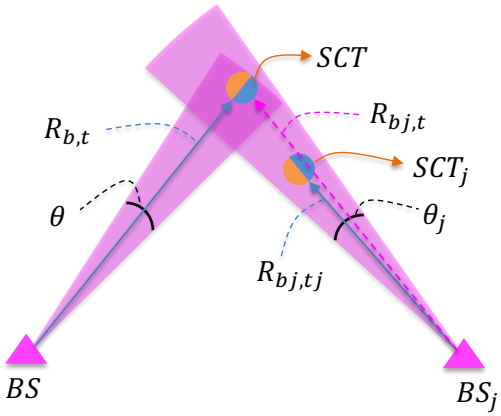

Fig. 5: Interfering model for downlink communication in JSAC

Based on the structure in Fig. 5, we can have the interference probability of BS_j, which is the probability of the signal transmitted from BS_j to its desired target SCT_j makes an interference at SCT, shown as:

$$A_{c,j} = \frac{\theta_j}{2\pi} = \frac{\arctan(\frac{C_d}{2R_{bj,tj}})}{\pi}, \tag{17}$$

where θ_j is the beamwidth of the j-th interfering BS.

Hence, we can have interference in the communication link as

$$I_c = \sum_{j=1,2,\cdots} P_{c,r,j}(R_{bj,t}), \tag{18}$$

where $P_{c,r,j}(R_{bj,t})$ is the received interference power of the j-th interfering BS, which is a function of the distance between the interfering BS BS_j and SCT.

D. Allocation of energy and spectrum between sensing and communication

Transmit power allocation,

$$P_t = P_{s,t} + P_{c,t} = \eta P_t + (1-\eta)P_t \tag{19}$$

Bandwidth allocation, Yehlex Tournament

$$B = B_s + B_c = \mu B + (1-\mu)B \tag{20}$$

IV. ANALYSIS OF INTEGRATED COVERAGE PROBABILITY IN JOINT SENSING AND COMMUNICATION

$$\mathbb{P}_{\text{j,cov}} = \mathbb{P}\big[\texttt{SCNR}_s \geq \tau_s, D_{s,res} \leq d'_{s,res}, \texttt{SINR}_c \geq \tau_c\big], \tag{21}$$

where $\tau_c = 2^{\frac{r_{c,com}}{B_c}} - 1$, and $r_{c,com}$ is the given minimum data rate in communication.

$$\mathbb{P}_{\text{j,cov}} = \mathbb{P}\big[\texttt{SCNR}_s \geq \tau_s, D_{s,res} \leq d'_{s,res}, \texttt{SINR}_c \geq \tau_c\big], \tag{22}$$

All the BSs and targets (ST, CST) are subject to PPP, with densities of γ_{bs}, γ_{st}, γ_{sct}.

Lemma 1. *According to the well-known theorem of PPP [18], [19], the PDF of the nearest distance in the homogeneous PPP is*

$$f_{R_{b,t}}(r_{b,t}) = 2\pi\gamma_{bs} r_{b,t} \exp(-\pi\gamma_{bs} r_{b,t}^2). \tag{23}$$

A. Analysis of the sensing link

$$\begin{aligned}
P_{s,\text{cov}} &= \mathbb{P}[\texttt{SCNR}_s > \tau_s] = \mathbb{P}\Big[\frac{P_{s,r}(D_{t,b})}{C_s + KT_0B_sF_n} > \tau_s\Big] = \mathbb{P}\Big[\frac{\frac{P_{s,t}g_{s,t}}{4\pi D_{t,b}^2} \times \frac{\rho_{st}}{4\pi D_{t,b}^2} \times \frac{g_{s,r}c^2}{4\pi f_s^2} \times NT_cH_s}{C_s + KT_0B_sF_n} > \tau_s\Big] \\
&= \mathbb{E}_{D_{t,b}}\Big[\mathbb{P}\Big[\frac{\frac{P_{s,t}g_{s,t}}{4\pi D_{t,b}^2} \times \frac{\rho_{st}}{4\pi D_{t,b}^2} \times \frac{g_{s,r}c^2}{4\pi f_s^2} \times NT_cH_s}{C_s + KT_0B_sF_n} > \tau_s \Big| D_{t,b} = d_{t,b}\Big]\Big] \\
&= \int_0^{d_{t,b}^{\max}} \mathbb{P}\Big[\frac{\frac{P_{s,t}g_{s,t}}{4\pi d_{t,b}^2} \times \frac{\rho_{st}}{4\pi d_{t,b}^2} \times \frac{g_{s,r}c^2}{4\pi f_s^2} \times NT_cH_s}{C_s + KT_0B_sF_n} > \tau_s\Big] f_{D_{t,b}}(d_{t,b})\mathrm{d}d_{t,b} \\
&= \int_0^{d_{t,b}^{\max}} \mathbb{P}\Big[H_s > \frac{\tau_s(C_s + KT_0B_sF_n)}{\frac{P_{s,t}g_{s,t}g_{s,r}\rho_{st}c^2}{(4\pi)^3 f_s^2} d_{t,b}^{-4} NT_c}\Big] 2\pi\gamma_{bs} d_{t,b} \exp(-\pi\gamma_{bs} d_{t,b}^2)\mathrm{d}d_{t,b},
\end{aligned} \tag{24}$$

where $P_{s,t}$ is the transmit power for sensing, $D_{t,b}$ is the distance between ST and BS, $g_{s,t}$ and $g_{s,r}$ are gains of the transmitting and the receiving antennas, $c = 3 \times 10^8$ m/s is the light speed, ρ_{st} is the radar cross section (RCS) on the ST, f_s is the center frequency of chirp ramp, N is the number of the transmitted chirps in a frame, T_c is the duration time of the chirp which is made by the frequency-modulated continuous-wave (FMCW) radar, K is the Boltzmann constant, T_0 is the standard temperature, B_s is the bandwidth for sensing, F_n is the noise figure, C_s is the total clutter signal power, τ_s is the threshold for the target sensing.

According the fact that $H_s \sim \exp(1)$, the inner probability term of (24) can be futher simplified as

$$\begin{aligned}
&\mathbb{P}\Big[H_s > \frac{\tau_s(C_s + KT_0B_sF_n)}{\frac{P_{s,t}g_{s,t}g_{s,r}\rho_{st}c^2}{(4\pi)^3 f_s^2} d_{t,b}^{-4} NT_c} \Big| d_{t,b}\Big] \\
&= \mathbb{E}_{C_s}\Big[\mathbb{P}\Big[H_s > \frac{\tau_s(C_s + KT_0B_sF_n)}{\frac{P_{s,t}g_{s,t}g_{s,r}\rho_{st}c^2}{(4\pi)^3 f_s^2} d_{t,b}^{-4} NT_c} \Big| C_s, d_{t,b}\Big]\Big] \\
&= \mathbb{E}_{C_s}\Big[\exp\Big(-\tau_s(C_s + KT_0B_sF_n)P_{s,t}^{-1}g_{s,t}^{-1}g_{s,r}^{-1}\rho_{st}^{-1}c^{-2}N^{-1}T_c^{-1}(4\pi)^3 f_s^2 d_{t,b}^4\Big)\Big] \\
&= \mathbb{E}_{C_{s,1},C_{s,2}}\Big[\exp\Big(-\tau_s(C_{s,1} + C_{s,2} + KT_0B_sF_n)P_{s,t}^{-1}g_{s,t}^{-1}g_{s,r}^{-1}\rho_{st}^{-1}c^{-2}N^{-1}T_c^{-1}(4\pi)^3 f_s^2 d_{t,b}^4\Big)\Big] \\
&= \exp\Big(-\tau_s KT_0B_sF_nP_{s,t}^{-1}g_{s,t}^{-1}g_{s,r}^{-1}\rho_{st}^{-1}c^{-2}N^{-1}T_c^{-1}(4\pi)^3 f_s^2 d_{t,b}^4\Big) \\
&\quad \times \exp\Big(-\tau_s C_{s,1}P_{s,t}^{-1}g_{s,t}^{-1}g_{s,r}^{-1}\rho_{st}^{-1}c^{-2}N^{-1}T_c^{-1}(4\pi)^3 f_s^2 d_{t,b}^4\Big) \\
&\quad \times \exp\Big(-\tau_s C_{s,2}P_{s,t}^{-1}g_{s,t}^{-1}g_{s,r}^{-1}\rho_{st}^{-1}c^{-2}N^{-1}T_c^{-1}(4\pi)^3 f_s^2 d_{t,b}^4\Big) \\
&= \exp\Big(-\tau_s KT_0B_sF_nP_{s,t}^{-1}g_{s,t}^{-1}g_{s,r}^{-1}\rho_{st}^{-1}c^{-2}N^{-1}T_c^{-1}(4\pi)^3 f_s^2 d_{t,b}^4\Big) \\
&\quad \times \mathcal{L}_{C_{s,1}}\Big(\tau_s P_{s,t}^{-1}g_{s,t}^{-1}g_{s,r}^{-1}\rho_{st}^{-1}c^{-2}N^{-1}T_c^{-1}(4\pi)^3 f_s^2 d_{t,b}^4\Big) \\
&\quad \times \mathcal{L}_{C_{s,2}}\Big(\tau_s P_{s,t}^{-1}g_{s,t}^{-1}g_{s,r}^{-1}\rho_{st}^{-1}c^{-2}N^{-1}T_c^{-1}(4\pi)^3 f_s^2 d_{t,b}^4\Big),
\end{aligned} \tag{25}$$

where $\mathcal{L}_{C_s}(\cdot)$ is the clutter Laplace tranform. We can calculate $\mathcal{L}_{C_s}(\cdot)$ as follows.

In the following, we will calculate the Laplace transform of $C_{s,1}$ and $C_{s,2}$ separately where $C_{s,1}$ and $C_{s,2}$ are shown in (15).

1) : Take the Laplace transform over $C_{s,1}$

$$\begin{aligned}
&\mathcal{L}_{C_{s,1}}(s) = \mathbb{E}\big[\exp(-sC_{s,1})\big|D_{t,b} = d_{t,b}\big] \\
&= \mathbb{E}\Big[\exp\Big(-s\sum_{j=1,2,\cdots}\big(\frac{P_{s,t}g_{s,t}}{4\pi D_{bj,t}^2}\frac{\rho_{st}}{4\pi D_{t,b}^2}\frac{g_{s,r}\lambda^2}{4\pi}NT_cH_{s,j}\big)\Big)\Big|D_{t,b} = d_{t,b}\Big] \\
&= \mathbb{E}\Big[\prod_{j=1,2,\cdots}\exp\Big(-s\times\frac{P_{s,t}g_{s,t}}{4\pi D_{bj,t}^2}\frac{\rho_{st}}{4\pi D_{t,b}^2}\frac{g_{s,r}\lambda^2}{4\pi}NT_cH_{s,j}\Big)\Big|D_{t,b} = d_{t,b}\Big]
\end{aligned} \tag{26}$$

Based on the fact that $H_{s,j}, j = 1, 2, \cdots$ are independent, we can move the expectation with respect to $H_{s,j}$ inside the multiplication, and we can have

$$\mathcal{L}_{C_{s,1}}(s) = \mathbb{E}\Big[\prod_{j=1,2,\cdots}\mathbb{E}_{H_{s,c1}}\Big[\exp\Big(-s\times\frac{P_{s,t}g_{s,t}}{4\pi D_{bj,t}^2}\frac{\rho_{st}}{4\pi D_{t,b}^2}\frac{g_{s,r}\lambda^2}{4\pi}NT_cH_{s,c1}\Big)\Big|D_{t,b} = d_{t,b}\Big]\Big]. \tag{27}$$

Lemma 2. *Probability generating functionl (PGFL)*

The PGFL [18] of a homogeneous PPP is given as

$$\mathcal{P}_{\Phi}(f)=\mathbb{E}\Big[\prod_{\mathbf{X}_i\in\Phi} f(\mathbf{X}_i)\Big]=\exp\Big(-\gamma\int_{\mathbb{R}^d}(1-f(\mathrm{x}))\mathrm{dx}\Big),$$

where γ is the density of the homogeneous PPP.

Based on the PGFL of PPP in Lemma 2, with respect to the function $f(\mathrm{x})=\mathbb{E}_{H_{s,c1}}\Big[\exp\big(-s\times\frac{P_{s,t}g_{s,t}}{4\pi D_{bj,t}^2}\frac{\rho_{st}}{4\pi D_{t,b}^2}\frac{g_{s,r}\lambda^2}{4\pi}NT_cH_{s,c1}\big)\Big|D_{t,b}=d_{t,b}\Big]$, we can get

$$\begin{aligned}&\mathcal{L}_{C_{s,1}}(s)\\&=\exp\Big(-\gamma_{bs}\int_{\mathbb{R}^{D_{bj,t}}}\Big(1-\mathbb{E}_{H_{s,c1}}\Big[\exp\big(-s\times\frac{P_{s,t}g_{s,t}}{4\pi d_{bj,t}^2}\frac{\rho_{st}}{4\pi D_{t,b}^2}\frac{g_{s,r}\lambda^2}{4\pi}NT_cH_{s,c1}\big)\Big|D_{t,b}=d_{t,b}\Big]\Big)\mathrm{d}d_{bj,t}\Big).\end{aligned}\tag{28}$$

Since we know that the distance between the BS_j and ST is bigger than the distance between BS and ST, $D_{bj,t}\geq D_{b,t}$. Employing a transformation to polar coordinates, we can get

$$\begin{aligned}&\mathcal{L}_{C_{s,1}}(s)\\&=\exp\Big(-2\pi\gamma_{bs}\int_{d_{b,t}}^{d_{bj,t}^{\max}}\Big(1-\mathbb{E}_{H_{s,c1}}\Big[\exp\big(-s\times\frac{P_{s,t}g_{s,t}}{4\pi d_{bj,t}^2}\frac{\rho_{st}}{4\pi d_{t,b}^2}\frac{g_{s,r}\lambda^2}{4\pi}NT_cH_{s,c1}\big)\Big|d_{t,b}\Big]\Big)d_{bj,t}\mathrm{d}d_{bj,t}\Big).\end{aligned}\tag{29}$$

Lemma 3. *The moment-generating function (MGF) of an exponential random variable*

The MGF of a real-valued random variable X *is [20]*

$$\mathbf{M}_{\mathrm{X}}(t)=\mathbb{E}[\mathrm{e}^{t\mathrm{x}}].\tag{30}$$

Since $\mathrm{X}\sim\exp(\beta)$ *and* $f_{\mathrm{X}}(x)=\frac{1}{\beta}\exp(-\frac{x}{\beta})$*, the MGF of the exponential random variable can be calculated as*

$$\begin{aligned}\mathbf{M}_{\mathrm{X}}(t)=\mathbb{E}[\mathrm{e}^{t\mathrm{x}}]&=\int_0^{\infty}\mathrm{e}^{tx}\frac{1}{\beta}\mathrm{e}^{-\frac{x}{\beta}}\mathrm{d}x\\&=\frac{1}{\beta}\int_0^{\infty}\mathrm{e}^{(t-\frac{1}{\beta})x}\mathrm{d}x=\frac{1}{\beta}\frac{1}{t-\frac{1}{\beta}}\Big[\mathrm{e}^{(t-\frac{1}{\beta})x}\Big]_0^{\infty}=\frac{1}{1-\beta t}.\end{aligned}\tag{31}$$

Based on Lemma 3, since $H_{s,j}\sim\exp(1)$, the moment generating function of an exponential random variable can be achieved and $\mathcal{L}_{C_{s,1}}(s)$ can be calculated as

$$\mathcal{L}_{C_{s,1}}(s)=\exp\Big(-2\pi\gamma_{bs}\int_{d_{b,t}}^{d_{bj,t}^{\max}}\Big(1-\mathbb{E}_{H_{s,c1}}\Big[\exp\big(-s\times\frac{P_{s,t}g_{s,t}}{4\pi d_{bj,t}^2}\frac{\rho_{st}}{4\pi d_{t,b}^2}\frac{g_{s,r}\lambda^2}{4\pi}NT_cH_{s,c1}\big)\Big|d_{t,b}\Big]\Big)d_{bj,t}\mathrm{d}d_{bj,t}\Big)$$

$$= \exp\Big(-2\pi\gamma_{bs} \int_{d_{b,t}}^{d_{bj,t}^{\max}} \Big(1 - \frac{1}{1 + s \times \frac{P_{s,t} g_{s,t}}{4\pi d_{bj,t}^2} \frac{\rho_{st}}{4\pi d_{t,b}^2} \frac{g_{s,r}\lambda^2}{4\pi} N T_c}\Big) d_{bj,t} \mathrm{d} d_{bj,t}\Big)$$

$$= \exp\Big(-2\pi\gamma_{bs} \int_{d_{b,t}}^{d_{bj,t}^{\max}} \Big(\frac{1}{1 + s^{-1} \times (\frac{P_{s,t} g_{s,t}}{4\pi d_{bj,t}^2} \frac{\rho_{st}}{4\pi d_{t,b}^2} \frac{g_{s,r}\lambda^2}{4\pi} N T_c)^{-1}}\Big) d_{bj,t} \mathrm{d} d_{bj,t}\Big). \tag{32}$$

Hence, we can have the Laplace transform over $C_{s,1}$ in (25) as

$$\mathcal{L}_{C_{s,1}}\Big(\tau_s P_{s,t}^{-1} g_{s,t}^{-1} g_{s,r}^{-1} \rho_{st}^{-1} c^{-2} N^{-1} T_c^{-1} (4\pi)^3 f_s^2 d_{t,b}^4\Big) = \exp\Big(-2\pi\gamma_{bs} \int_{d_{b,t}}^{d_{bj,t}^{\max}} \Big(\frac{\tau_s}{\tau_s + (\frac{d_{bj,t}}{d_{t,b}})^2}\Big) d_{bj,t} \mathrm{d} d_{bj,t}\Big). \tag{33}$$

2) : Take the Laplace transform over $C_{s,2}$

$$\mathcal{L}_{C_{s,2}}(s) = \mathbb{E}\big[\exp(-sC_{s,2}) \big| D_{t,b} = d_{t,b}\big]$$

$$= \mathbb{E}\Big[\exp\Big(-s \sum_{i=1,2,\cdots} \big(\frac{P_{s,t} g_{s,t}}{4\pi D_{b,ti}^2} \frac{\rho_{st,i}}{4\pi D_{ti,t}^2} \frac{\rho_{st}}{4\pi D_{t,b}^2} \frac{g_{s,r}\lambda^2}{4\pi} N T_c H_{s,i}\big)\Big) \Big| D_{t,b} = d_{t,b}\Big]$$

$$= \mathbb{E}\Big[\prod_{i=1,2,\cdots} \exp\Big(-s \times \frac{P_{s,t} g_{s,t}}{4\pi D_{b,ti}^2} \frac{\rho_{st,i}}{4\pi D_{ti,t}^2} \frac{\rho_{st}}{4\pi D_{t,b}^2} \frac{g_{s,r}\lambda^2}{4\pi} N T_c H_{s,i}\Big) \Big| D_{t,b} = d_{t,b}\Big] \tag{34}$$

Based on the fact that $H_{s,i}, i = 1, 2, \cdots$ are independent, we can move the expectation with respect to $H_{s,i}$ inside the multiplication, and we can have

$$\mathcal{L}_{C_{s,2}}(s) = \mathbb{E}\Big[\prod_{i=1,2,\cdots} \mathbb{E}_{H_{s,c2}}\Big[\exp\Big(-s \times \frac{P_{s,t} g_{s,t}}{4\pi D_{b,ti}^2} \frac{\rho_{st,i}}{4\pi D_{ti,t}^2} \frac{\rho_{st}}{4\pi D_{t,b}^2} \frac{g_{s,r}\lambda^2}{4\pi} N T_c H_{s,c2}\Big) \Big| D_{t,b} = d_{t,b}\Big]\Big]. \tag{35}$$

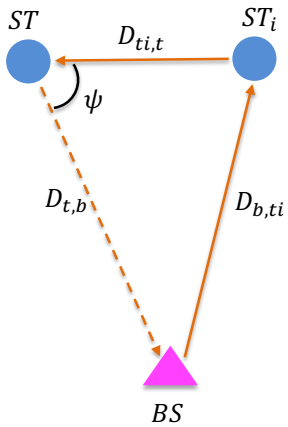

Fig. 6: Relationships between $D_{b,ti}$, $D_{ti,t}$, $D_{t,b}$, and ψ

As shown in Fig. 6, we can have the relationship between $D_{b,ti}$, $D_{ti,t}$, and $D_{t,b}$ as

$$D_{b,ti}^2 = D_{t,b}^2 + D_{ti,t}^2 - 2D_{t,b}D_{ti,t}\cos(\psi) \tag{36}$$

where $D_{t,b}$ and ψ are independent and

$$\begin{cases} f_{D_{t,b}}(d_{t,b}) = 2\pi\gamma_{bs} d_{t,b} \exp(-\pi\gamma_{bs} d_{t,b}^2) \\ f(\psi) = \frac{1}{2\pi},\ 0 \le \psi \le 2\pi \end{cases} \tag{37}$$

Hence, we can have

$$\begin{aligned} &\mathcal{L}_{C_{s,2}}(s) \\ &= \mathbb{E}\Big[\prod_{i=1,2,\cdots} \mathbb{E}_{H_{s,c2}}\Big[\exp\Big(- s \times \frac{P_{s,t} g_{s,t}}{4\pi(d_{t,b}^2 + D_{ti,t}^2 - 2d_{t,b} D_{ti,t}\cos(\psi))} \frac{\rho_{st,i}}{4\pi D_{ti,t}^2} \frac{\rho_{st}}{4\pi d_{t,b}^2} \frac{g_{s,r}\lambda^2}{4\pi} N T_c H_{s,c2}\Big) \Big| d_{t,b}, \psi \Big]\Big]. \end{aligned} \tag{38}$$

Using the PGFL of PPP in Lemma 2 with respect to the function $f(\mathrm{x}) = \mathbb{E}_{H_{s,c2}}\Big[\exp\Big(- s \times \frac{P_{s,t} g_{s,t}}{4\pi(d_{t,b}^2 + D_{ti,t}^2 - 2d_{t,b} D_{ti,t}\cos(\psi))} \frac{\rho_{st,i}}{4\pi D_{ti,t}^2} \frac{\rho_{st}}{4\pi d_{t,b}^2} \frac{g_{s,r}\lambda^2}{4\pi} N T_c H_{s,c2}\Big) \Big| d_{t,b}, \psi \Big]$, we can get

$$\begin{aligned} &\mathcal{L}_{C_{s,2}}(s) \\ &= \exp\Big(- \gamma_{st} \int_{\mathbb{R}^{D_{ti,t}}} \Big(1 - \mathbb{E}_{H_{s,c2}}\Big[\exp\Big(- s \times \frac{P_{s,t} g_{s,t}}{4\pi(d_{t,b}^2 + d_{ti,t}^2 - 2d_{t,b} d_{ti,t}\cos(\psi))} \frac{\rho_{st,i}}{4\pi d_{ti,t}^2} \frac{\rho_{st}}{4\pi d_{t,b}^2} \frac{g_{s,r}\lambda^2}{4\pi} N T_c H_{s,c2}\Big) \Big| d_{t,b}, \psi \Big]\Big) \mathrm{d}d_{ti,t}\Big) \\ &= \exp\Big(- \gamma_{st} \int_0^{d_{ti,t}^{\max}} \Big(1 - \mathbb{E}_{H_{s,c2}}\Big[\exp\Big(- s \times \frac{P_{s,t} g_{s,t}}{4\pi(d_{t,b}^2 + d_{ti,t}^2 - 2d_{t,b} d_{ti,t}\cos(\psi))} \frac{\rho_{st,i}}{4\pi d_{ti,t}^2} \frac{\rho_{st}}{4\pi d_{t,b}^2} \frac{g_{s,r}\lambda^2}{4\pi} N T_c H_{s,c2}\Big) \Big| d_{t,b}, \psi \Big]\Big) d_{ti,t} \mathrm{d}d_{ti,t}\Big). \end{aligned} \tag{39}$$

Based on Lemma 3, since $H_{s,i} \sim \exp(1)$, the moment generating function of an exponential random variable can be achieved and $\mathcal{L}_{C_{s,2}}(s)$ can be calculated as

$$\begin{aligned} &\mathcal{L}_{C_{s,2}}(s) \\ &= \exp\Big(- \gamma_{st} \int_0^{\infty} \Big(1 - \mathbb{E}_{H_{s,c2}}\Big[\exp\Big(- s \times \frac{P_{s,t} g_{s,t}}{4\pi(d_{t,b}^2 + d_{ti,t}^2 - 2d_{t,b} d_{ti,t}\cos(\psi))} \frac{\rho_{st,i}}{4\pi d_{ti,t}^2} \frac{\rho_{st}}{4\pi d_{t,b}^2} \frac{g_{s,r}\lambda^2}{4\pi} N T_c H_{s,c2}\Big) \Big| d_{t,b}, \psi \Big]\Big) d_{ti,t} \mathrm{d}d_{ti,t}\Big) \\ &= \exp\Big(- \gamma_{st} \int_0^{2\pi} \int_0^{d_{ti,t}^{\max}} \Big(1 - \frac{1}{1 + s \times \frac{P_{s,t} g_{s,t}}{4\pi(d_{t,b}^2 + d_{ti,t}^2 - 2d_{t,b} d_{ti,t}\cos(\psi))} \frac{\rho_{st,i}}{4\pi d_{ti,t}^2} \frac{\rho_{st}}{4\pi d_{t,b}^2} \frac{g_{s,r}\lambda^2}{4\pi} N T_c}\Big) d_{ti,t} \mathrm{d}d_{ti,t} \mathrm{d}\psi\Big) \\ &= \exp\Big(- \gamma_{st} \int_0^{2\pi} \int_0^{d_{ti,t}^{\max}} \Big(\frac{1}{1 + s^{-1} \times (\frac{P_{s,t} g_{s,t}}{4\pi(d_{t,b}^2 + d_{ti,t}^2 - 2d_{t,b} d_{ti,t}\cos(\psi))} \frac{\rho_{st,i}}{4\pi d_{ti,t}^2} \frac{\rho_{st}}{4\pi d_{t,b}^2} \frac{g_{s,r}\lambda^2}{4\pi} N T_c)^{-1}}\Big) d_{ti,t} \mathrm{d}d_{ti,t} \mathrm{d}\psi\Big). \end{aligned} \tag{40}$$

Hence, we can have the Laplace transform over $C_{s,2}$ in (25) as

$$\begin{aligned} &\mathcal{L}_{C_{s,2}}\Big(\tau_s P_{s,t}^{-1} g_{s,t}^{-1} g_{s,r}^{-1} \rho_{st}^{-1} c^{-2} N^{-1} T_c^{-1} (4\pi)^3 f_s^2 d_{t,b}^4\Big) \\ &= \exp\Big(- \gamma_{st} \int_0^{2\pi} \int_0^{d_{ti,t}^{\max}} \Big(\frac{\tau_s}{\tau_s + \frac{4\pi d_{ti,t}^2 (d_{t,b}^2 + d_{ti,t}^2 - 2d_{t,b} d_{ti,t}\cos(\psi))}{\rho_{st,i} d_{t,b}^2}}\Big) d_{ti,t} \mathrm{d}d_{ti,t} \mathrm{d}\psi\Big). \end{aligned} \tag{41}$$

Using the Laplace transform over $C_{s,1}$ and $C_{s,2}$ in (33) and (41), we can calculate (25) as

$$\begin{aligned}
&\mathbb{P}\Big[H_s > \frac{\tau_s(C_s+KT_0B_sF_n)}{\frac{P_{s,t}g_{s,t}g_{s,r}\rho_{st}c^2}{(4\pi)^3f_s^2}d_{t,b}^{-4}NT_c}\Big|d_{t,b}\Big]\\
&=\exp\Big(-\tau_sKT_0B_sF_nP_{s,t}^{-1}g_{s,t}^{-1}g_{s,r}^{-1}\rho_{st}^{-1}c^{-2}N^{-1}T_c^{-1}(4\pi)^3f_s^2d_{t,b}^4\Big)\\
&\quad\times\exp\Big(-2\pi\gamma_{bs}\int_{d_{b,t}}^{d_{bj,t}^{\max}}\Big(\frac{\tau_s}{\tau_s+(\frac{d_{bj,t}}{d_{t,b}})^2}\Big)d_{bj,t}\mathrm{d}d_{bj,t}\Big)\\
&\quad\times\exp\Big(-\gamma_{st}\int_0^{2\pi}\int_0^{d_{ti,t}^{\max}}\Big(\frac{\tau_s}{\tau_s+\frac{4\pi d_{ti,t}^2(d_{t,b}^2+d_{ti,t}^2-2d_{t,b}d_{ti,t}\cos(\psi))}{\rho_{st,i}d_{t,b}^2}}\Big)d_{ti,t}\mathrm{d}d_{ti,t}\mathrm{d}\psi\Big).
\end{aligned}\tag{42}$$

Take (42) into (24), and we can have the final expression of the coverage probability of the sensing link in JASC.

Theorem 1. *The probability of coverage of the downlink sensing in JSAC is*

$$\begin{aligned}
P_{s,\mathrm{cov}}&=\mathbb{P}[\mathtt{SCNR}_s>\tau_s]\\
&=\int_0^{d_{t,b}^{\max}}\mathbb{P}\Big[H_s>\frac{\tau_s(C_s+KT_0B_sF_n)}{\frac{P_{s,t}g_{s,t}g_{s,r}\rho_{st}c^2}{(4\pi)^3f_s^2}d_{t,b}^{-4}NT_c}\Big]2\pi\gamma_{bs}d_{t,b}\exp(-\pi\gamma_{bs}d_{t,b}^2)\mathrm{d}d_{t,b}\\
&=\int_0^{d_{t,b}^{\max}}\Big(\exp\Big(-\tau_sKT_0B_sF_nP_{s,t}^{-1}g_{s,t}^{-1}g_{s,r}^{-1}\rho_{st}^{-1}c^{-2}N^{-1}T_c^{-1}(4\pi)^3f_s^2d_{t,b}^4\Big)\\
&\qquad\times\exp\Big(-2\pi\gamma_{bs}\int_{d_{b,t}}^{d_{bj,t}^{\max}}\Big(\frac{\tau_s}{\tau_s+(\frac{d_{bj,t}}{d_{t,b}})^2}\Big)d_{bj,t}\mathrm{d}d_{bj,t}\Big)\\
&\qquad\times\exp\Big(-\gamma_{st}\int_0^{2\pi}\int_0^{d_{ti,t}^{\max}}\Big(\frac{\tau_s}{\tau_s+\frac{4\pi d_{ti,t}^2(d_{t,b}^2+d_{ti,t}^2-2d_{t,b}d_{ti,t}\cos(\psi))}{\rho_{st,i}d_{t,b}^2}}\Big)d_{ti,t}\mathrm{d}d_{ti,t}\mathrm{d}\psi\Big)\\
&\qquad\times2\pi\gamma_{bs}d_{t,b}\exp(-\pi\gamma_{bs}d_{t,b}^2)\Big)\mathrm{d}d_{t,b}.
\end{aligned}\tag{43}$$

B. Analysis of the communication link

Based on the communication channel in (12), the coverage probability of the downlink communication in JSAC between the tagged BS and the target at a random distance $R_{b,t}$ is

$$\begin{aligned}
P_{c,\mathrm{cov}}&=\mathbb{P}[\mathtt{SINR}_c>\tau_c]=\mathbb{P}\Big[\frac{P_{c,r}(R_{b,t})H_cg_{c,b}}{N_0B_c+I_c}>\tau_c\Big]=\mathbb{P}\Big[\frac{\frac{P_{c,t}\times10^{2.8}}{f_c^2R_{b,t}^{1.9}\times10^{0.1L_{sum}}}H_cg_{c,b}}{N_0B_c+I_c}>\tau_c\Big]\\
&=\mathbb{E}_{R_{b,t}}\Big[\mathbb{P}\Big[\frac{\frac{P_{c,t}\times10^{2.8}}{f_c^2R_{b,t}^{1.9}\times10^{0.1L_{sum}}}H_cg_{c,b}}{N_0B_c+I_c}>\tau_c\Big|R_{b,t}=r_{b,t}\Big]\Big]
\end{aligned}$$

$$= \int_0^{r_{b,t}^{\max}} \mathbb{P}\Big[\frac{\frac{P_{c,t}\times 10^{2.8}}{f_c^2 r_{b,t}^{1.9}\times 10^{0.1L_{sum}}} H_c g_{c,b}}{N_0 B_c + I_c} > \tau_c\Big] f_{R_{b,t}}(r_{b,t})\mathrm{d}r_{b,t}$$

$$= \int_0^{r_{b,t}^{\max}} \mathbb{P}\big[H_c > \tau_c(N_0 B_c + I_c) f_c^2 r_{b,t}^{1.9} P_{c,t}^{-1} g_{c,b}^{-1} 10^{(0.1L_{sum}-2.8)}\big] f_{R_{b,t}}(r_{b,t})\mathrm{d}r_{b,t}, \tag{44}$$

where $P_{c,t}$ is the transmit power of communication, $R_{b,t}$ is the communication range between BS and SCT, H_c is the fading exponent of the channel, H_c is the exponential factor, $g_{c,b} = 10^{0.1G_{c,b}}$ where $G_{c,b}$ is the beamforming gain of communication in dB, f_c is the signal frequency, N_0 is the power spectral density of noise in communication, B_c is the bandwidth used for communication, I_c is the total interference power, τ_c is the threshold to achieve communictaion.

According the fact that $H_c \sim \exp(1)$, the inner probability term of (44) can be futher simplified as

$$\begin{aligned}
&\mathbb{P}\big[H_c > \tau_c(N_0 B_c + I_c) f_c^2 r_{b,t}^{1.9} P_{c,t}^{-1} g_{c,b}^{-1} 10^{(0.1L_{sum}-2.8)} | r_{b,t}\big] \\
&= \mathbb{E}_{I_c}\Big[\mathbb{P}\big[H_c > \tau_c(N_0 B_c + I_c) f_c^2 r_{b,t}^{1.9} P_{c,t}^{-1} g_{c,b}^{-1} 10^{(0.1L_{sum}-2.8)} | I_c, r_{b,t}\big]\Big] \\
&= \mathbb{E}_{I_c}\big[\exp\big(-\tau_c(N_0 B_c + I_c) f_c^2 r_{b,t}^{1.9} P_{c,t}^{-1} g_{c,b}^{-1} 10^{(0.1L_{sum}-2.8)}\big) | r_{b,t}\big] \\
&= \exp\big(-\tau_c N_0 B_c f_c^2 r_{b,t}^{1.9} P_{c,t}^{-1} g_{c,b}^{-1} 10^{(0.1L_{sum}-2.8)}\big)\mathbb{E}_{I_c}\big[\exp\big(-\tau_c I_c f_c^2 r_{b,t}^{1.9} P_{c,t}^{-1} g_{c,b}^{-1} 10^{(0.1L_{sum}-2.8)}\big)\big] \\
&= \exp\big(-\tau_c N_0 B_c f_c^2 r_{b,t}^{1.9} P_{c,t}^{-1} g_{c,b}^{-1} 10^{(0.1L_{sum}-2.8)}\big)\mathcal{L}_{I_c}\big(\tau_c f_c^2 r_{b,t}^{1.9} P_{c,t}^{-1} g_{c,b}^{-1} 10^{(0.1L_{sum}-2.8)}\big),
\end{aligned} \tag{45}$$

where $\mathcal{L}_{I_c}(\cdot)$ is the interference Laplace transform. We can calculate $\mathcal{L}_{I_c}(\cdot)$ as follows.

Based on the communication channel in (12), we can have

$$\begin{aligned}
I_c &= \sum_{j=1,2,\cdots} P_{c,r,j}(R_{bj,t}) = \sum_{j=1,2,\cdots} \frac{P_{c,t}\times 10^{2.8}}{f_c^2 R_{bj,t}^{1.9}\times 10^{0.1L_{sum}}} H_{c,j} g_{c,b} \\
&= \sum_{j=1,2,\cdots} 10^{(2.8-0.1L_{sum})} P_{c,t} f_c^{-2} R_{bj,t}^{-1.9} H_{c,j} g_{c,b}.
\end{aligned} \tag{46}$$

Take the Laplace transform over I_c, and we can get

$$\begin{aligned}
\mathcal{L}_{I_c}(s) &= \mathbb{E}[\exp(-sI_c)] = \mathbb{E}\Big[\exp\big(-s\sum_{j=1,2,\cdots} 10^{(2.8-0.1L_{sum})} P_{c,t} f_c^{-2} R_{bj,t}^{-1.9} H_{c,j} g_{c,b}\big)\Big] \\
&= \mathbb{E}\Big[\prod_{j=1,2,\cdots} \exp\big(-s\times 10^{(2.8-0.1L_{sum})} P_{c,t} f_c^{-2} R_{bj,t}^{-1.9} H_{c,j} g_{c,b}\big)\Big].
\end{aligned} \tag{47}$$

Based on the fact that $H_{c,j}, j = 1, 2, \cdots$ are independent, we can move the expectation with respect to $H_{c,j}$ inside the multiplication, and we can have

$$\mathcal{L}_{I_c}(s) = \mathbb{E}\Big[\prod_{j=1,2,\cdots} \mathbb{E}_{H_c}\Big[\exp\big(-s\times 10^{(2.8-0.1L_{sum})} P_{c,t} f_c^{-2} R_{bj,t}^{-1.9} H_c g_{c,b}\big)\Big]\Big]. \tag{48}$$

Considering the interference probability, $A_{c,j}$, which can be regarded as the impairment of

the BS's density. Based on Lemma 2, with respect to the function $f(\mathrm{x}) = \mathbb{E}_{H_c}\big[\exp\big(-s\times 10^{2.8-0.1L_{sum}}P_{c,t}f_c^{-2}R_{bj,t}^{-1.9}H_c g_{c,b}\big)\big]$, we can get

$$\begin{aligned}&\mathcal{L}_{I_c}(s)\\&=\exp\Bigg(-\gamma_{bs}A_{c,j}\int_{\mathbb{R}^{R_{bj,t}}}\Big(1-\mathbb{E}_{H_c}\Big[\exp\big(-s\times 10^{(2.8-0.1L_{sum})}P_{c,t}f_c^{-2}r_{bj,t}^{-1.9}H_c g_{c,b}\big)\Big]\Big)\mathrm{d}r_{bj,t}\Bigg).\end{aligned} \tag{49}$$

Since we know that the distance between the BS_j and SCT is bigger than the distance between BS and SCT, $R_{bj,t}\geq R_{b,t}$. Employing a transformation to polar coordinates, we can get

$$\begin{aligned}&\mathcal{L}_{I_c}(s)\\&=\exp\Bigg(-2\pi\gamma_{bs}A_{c,j}\int_{r_{b,t}}^{r_{bj,t}^{\max}}\Big(1-\mathbb{E}_{H_c}\Big[\exp\big(-s\times 10^{2.8-0.1L_{sum}}P_{c,t}f_c^{-2}r_{bj,t}^{-1.9}H_c g_{c,b}\big)\Big]\Big)r_{bj,t}\mathrm{d}r_{bj,t}\Bigg).\end{aligned} \tag{50}$$

Based on Lemma 3, since $H_{c,j}\sim\exp(1)$, the moment generating function of an exponential random variable can be achieved and $\mathcal{L}_{I_c}(s)$ can be calculated as

$$\begin{aligned}\mathcal{L}_{I_c}(s)&=\exp\Bigg(-2\pi\gamma_{bs}A_{c,j}\int_{r_{b,t}}^{r_{bj,t}^{\max}}\Big(1-\mathbb{E}_{H_c}\Big[\exp\big(-s\times 10^{2.8-0.1L_{sum}}P_{c,t}f_c^{-2}r_{bj,t}^{-1.9}H_c g_{c,b}\big)\Big]\Big)r_{bj,t}\mathrm{d}r_{bj,t}\Bigg)\\&=\exp\Bigg(-2\pi\gamma_{bs}A_{c,j}\int_{r_{b,t}}^{r_{bj,t}^{\max}}\Big(1-\frac{1}{1+s\times 10^{2.8-0.1L_{sum}}P_{c,t}f_c^{-2}r_{bj,t}^{-1.9}g_{c,b}}\Big)r_{bj,t}\mathrm{d}r_{bj,t}\Bigg)\\&=\exp\Bigg(-2\pi\gamma_{bs}A_{c,j}\int_{r_{b,t}}^{r_{bj,t}^{\max}}\Big(\frac{1}{1+s^{-1}(10^{2.8-0.1L_{sum}}P_{c,t}f_c^{-2}r_{bj,t}^{-1.9}g_{c,b})^{-1}}\Big)r_{bj,t}\mathrm{d}r_{bj,t}\Bigg).\end{aligned} \tag{51}$$

Hence, we can have the Laplace transform over I_c in (45) as

$$\mathcal{L}_{I_c}\big(\tau_c f_c^2 r_{b,t}^{1.9}P_{c,t}^{-1}g_{c,b}^{-1}10^{(0.1L_{sum}-2.8)}\big)=\exp\Bigg(-2\pi\gamma_{bs}A_{c,j}\int_{r_{b,t}}^{r_{bj,t}^{\max}}\Big(\frac{\tau_c}{\tau_c+(\frac{r_{bj,t}}{r_{b,t}})^{1.9}}\Big)r_{bj,t}\mathrm{d}r_{bj,t}\Bigg). \tag{52}$$

Using the Laplace transform over I_c in (51), we can calculate (45) as

$$\begin{aligned}&\mathbb{P}\big[H_c>\tau_c(N_0B_c+I_c)f_c^2r_{b,t}^{1.9}P_{c,t}^{-1}g_{c,b}^{-1}10^{(0.1L_{sum}-2.8)}|r_{b,t}\big]\\&=\exp\big(-\tau_cN_0B_cf_c^2r_{b,t}^{1.9}P_{c,t}^{-1}g_{c,b}^{-1}10^{(0.1L_{sum}-2.8)}\big)\times\mathcal{L}_{I_c}\big(\tau_cf_c^2r_{b,t}^{1.9}P_{c,t}^{-1}g_{c,b}^{-1}10^{(0.1L_{sum}-2.8)}\big)\\&=\exp\big(-\tau_cN_0B_cf_c^2r_{b,t}^{1.9}P_{c,t}^{-1}g_{c,b}^{-1}10^{(0.1L_{sum}-2.8)}\big)\times\exp\Bigg(-2\pi\gamma_{bs}A_{c,j}\int_{r_{b,t}}^{r_{bj,t}^{\max}}\Big(\frac{\tau_c}{\tau_c+(\frac{r_{bj,t}}{r_{b,t}})^{1.9}}\Big)r_{bj,t}\mathrm{d}r_{bj,t}\Bigg).\end{aligned} \tag{53}$$

Take the interference probability $A_{c,j}$ in (17) into consideration and take expectation over

$R_{bj,tj}$, we can have

$$\begin{aligned}
&\mathbb{P}\big[H_c > \tau_c(N_0B_c + I_c)f_c^2 r_{b,t}^{1.9} P_{c,t}^{-1} g_{c,b}^{-1} 10^{(0.1L_{sum}-2.8)} | r_{b,t}\big] \\
&= \exp\big(-\tau_c N_0 B_c f_c^2 r_{b,t}^{1.9} P_{c,t}^{-1} g_{c,b}^{-1} 10^{(0.1L_{sum}-2.8)}\big) \\
&\quad \times \int_0^{r_{bj,tj}^{\max}} \exp\Big(-2\pi\gamma_{bs}\frac{\arctan(\frac{C_d}{2r_{bj,tj}})}{\pi}\int_{r_{b,t}}^{r_{bj,t}^{\max}} \big(\frac{\tau_c}{\tau_c + (\frac{r_{bj,t}}{r_{b,t}})^{1.9}}\big) r_{bj,t}\mathrm{d}r_{bj,t}\Big) f_{R_{bj,tj}}(r_{bj,tj})\mathrm{d}r_{bj,tj},
\end{aligned} \tag{54}$$

where $f_{R_{bj,tj}}(r_{bj,tj}) = 2\pi\gamma_{sct} r_{bj,tj}\exp(-\pi\gamma_{sct} r_{bj,tj}^2)$.

Take (53) into (44), and we can have the final expression of the coverage probability of the communication link in JASC.

Theorem 2. *The probability of coverage of the downlink communication in JSAC is*

$$\begin{aligned}
P_{c,\mathrm{cov}} &= \mathbb{P}[\mathtt{SINR}_c > \tau_c] \\
&= \int_0^{r_{b,t}^{\max}} \mathbb{P}\big[H_c > \tau_c(N_0B_c + I_c)f_c^2 r_{b,t}^{1.9} P_{c,t}^{-1} g_{c,b}^{-1} 10^{(0.1L_{sum}-2.8)}\big] 2\pi\gamma_{bs} r_{b,t}\exp(-\pi\gamma_{bs} r_{b,t}^2)\mathrm{d}r_{b,t} \\
&= \int_0^{r_{b,t}^{\max}} \Bigg(\exp\big(-\tau_c N_0 B_c f_c^2 r_{b,t}^{1.9} P_{c,t}^{-1} g_{c,b}^{-1} 10^{(0.1L_{sum}-2.8)}\big) \\
&\quad \times \int_0^{r_{bj,tj}^{\max}} \exp\Big(-2\pi\gamma_{bs}\frac{\arctan(\frac{C_d}{2r_{bj,tj}})}{\pi}\int_{r_{b,t}}^{r_{bj,t}^{\max}} \big(\frac{\tau_c}{\tau_c + (\frac{r_{bj,t}}{r_{b,t}})^{1.9}}\big) r_{bj,t}\mathrm{d}r_{bj,t}\Big) f_{R_{bj,tj}}(r_{bj,tj})\mathrm{d}r_{bj,tj} \\
&\quad \times 2\pi\gamma_{bs} r_{b,t}\exp(-\pi\gamma_{bs} r_{b,t}^2)\Bigg)\mathrm{d}r_{b,t},
\end{aligned} \tag{55}$$

where $\tau_c = 2^{\frac{r_{c,com}}{B_c}} - 1$.

C. Constrain of the distance resolution in the sensing

Considering the distance resolution for the sensing:

$$D_{s,\mathrm{res}} = \frac{cT_c}{2B_s(T_c - \frac{2D_{t,b}}{c})} \le d'_{s,res} \;\Rightarrow\; D_{t,b} \le \frac{c}{2}\big(T_c - \frac{cT_c}{2B_s d'_{s,res}}\big) \tag{56}$$

D. Joint analysis of the sensing and communication links

$$\mathbb{P}_{\mathrm{j,cov}} = \mathbb{P}\Big[\mathtt{SCNR}_s \ge \tau_s, D_{t,b} \le \frac{c}{2}\big(T_c - \frac{cT_c}{2B_s d'_{s,res}}\big), \mathtt{SINR}_c \ge \tau_c\Big] \tag{57}$$

$$= \mathbb{P}\Big[\mathtt{SCNR}_s \times \mathbb{1}\big(D_{t,b} \le \frac{c}{2}(T_c - \frac{cT_c}{2B_s d'_{s,res}})\big) \ge \tau_s\Big] \times \mathbb{P}\Big[\mathtt{SINR}_c \ge \tau_c\Big] \tag{58}$$

$$= \int_0^{d'_{t,b}} \Big(\exp\big(-\tau_s K T_0 B_s F_n P_{s,t}^{-1} g_{s,t}^{-1} g_{s,r}^{-1} \rho_{st}^{-1} c^{-2} N^{-1} T_c^{-1} (4\pi)^3 f_s^2 d_{t,b}^4\big) \tag{59}$$

$$\times \exp\Big(-2\pi\gamma_{bs}\int_{d_{b,t}}^{d_{bj,t}^{\max}}\big(\frac{\tau_s}{\tau_s+(\frac{d_{bj,t}}{d_{t,b}})^2}\big)d_{bj,t}\mathrm{d}d_{bj,t}\Big)$$

$$\times \exp\Big(-\gamma_{st}\int_0^{2\pi}\int_0^{d_{ti,t}^{\max}}\big(\frac{\tau_s}{\tau_s+\frac{4\pi d_{ti,t}^2(d_{t,b}^2+d_{ti,t}^2-2d_{t,b}d_{ti,t}\cos(\psi))}{\rho_{st,i}d_{t,b}^2}}\big)d_{ti,t}\mathrm{d}d_{ti,t}\mathrm{d}\psi\Big)$$

$$\times 2\pi\gamma_{bs}d_{t,b}\exp(-\pi\gamma_{bs}d_{t,b}^2)\Big)\mathrm{d}d_{t,b}$$

$$\times\int_0^{r_{b,t}^{\max}}\Big(\exp\big(-\tau_c N_0 B_c f_c^2 r_{b,t}^{1.9}P_{c,t}^{-1}g_{c,b}^{-1}10^{(0.1L_{sum}-2.8)}\big) \tag{60}$$

$$\times\int_0^{r_{bj,tj}^{\max}}\exp\Big(-2\pi\gamma_{bs}\frac{\arctan(\frac{C_d}{2r_{bj,tj}})}{\pi}\int_{r_{b,t}}^{r_{bj,t}^{\max}}\big(\frac{\tau_c}{\tau_c+(\frac{r_{bj,t}}{r_{b,t}})^{1.9}}\big)r_{bj,t}\mathrm{d}r_{bj,t}\Big)f_{R_{bj,tj}}(r_{bj,tj})\mathrm{d}r_{bj,tj}$$

$$\times 2\pi\gamma_{bs}r_{b,t}\exp(-\pi\gamma_{bs}r_{b,t}^2)\Big)\mathrm{d}r_{b,t} \tag{61}$$

where $d'_{t,b}=\min\big(d_{t,b}^{\max},\frac{c}{2}(T_c-\frac{cT_c}{2B_s d'_{s,res}})\big)$, and $\tau_c=2^{\frac{r_{c,com}}{B_c}}-1$.

V. Simulation

abcd abcd abcd abcd abcd abcd abcd abcd abcd abcd abcd abcd abcd abcd abcd abcd abcd abcd abcd abcd abcd abcd abcd abcd abcdabcd abcd abcd abcd abcd abcd

TABLE I: Table of Notations and Abbreviations

Notation	Description	Value
P_t	The total transmit power	21 dBm [21]
B	The total bandwidth	4 GHz [21]
$\gamma_{bs}, \gamma_{st}, \gamma_{sct}$	Densities of BS, ST, and SCT	
$d'_{s,res}$	Maximum distance resolution in sensing	
C_d	The cover diameter	10 m
$g_{s,t}, g_{s,r}$	Antenna gains at transmitter and receiver	10 dB, 10 dB [21]
$\rho_{st}, \rho_{st,i}$	Radar cross section	0.5, 0.5
T_c, N	Duration time of the chirp signal, the number of chirps	40 ms, 100 [21]
F_n	Noise figure at the receive antenna in sensing	13 dB [21]
$r'_{c,com}$	Minimum data rate in communication	
$L_{gas} + L_{rain}$	Path loss for gas and rain	0.7 dB/km [13], [14]
L_{add}, L_{imp}	additional loss and implementation loss	20 dB, 5dB [16]
N_0	Noise power spectral density	-164 dB/Hz [16]
g_{cb}	Beamforming gain in communication	29.2 dB [22]

In Fig. 7(a), we have the particular parameters as

VI. Conclusion

abcd abcd abcd abcd abcd abcd abcd abcd abcd abcd abcd abcd abcd abcd abcd abcd abcd abcd abcd abcd abcd abcd abcd abcd abcd abcd abcd abcd abcd abcd abcd abcd abcd abcd abcd abcd abcd abcd abcd abcd abcd abcd

TABLE II: Parameters used in simulation

(a) Parameters for Fig. 7(a)

Notation	Value
$\gamma_{st}, \gamma_{sct}$	300, 300 (points/km^2)
$d'_{s,res}$	0.2 m
τ_s	0.01
$r'_{c,com}$	0.5 Gbps
μ, η	0.5, 0.5

(b) Parameters for Fig. 7(b)

Notation	Value
$d'_{s,res}$	13
γ_{bs}	50 (points/km^2)
$\gamma_{st}, \gamma_{sct}$	300, 300 (points/km^2)
μ, η	0.5, 0.5

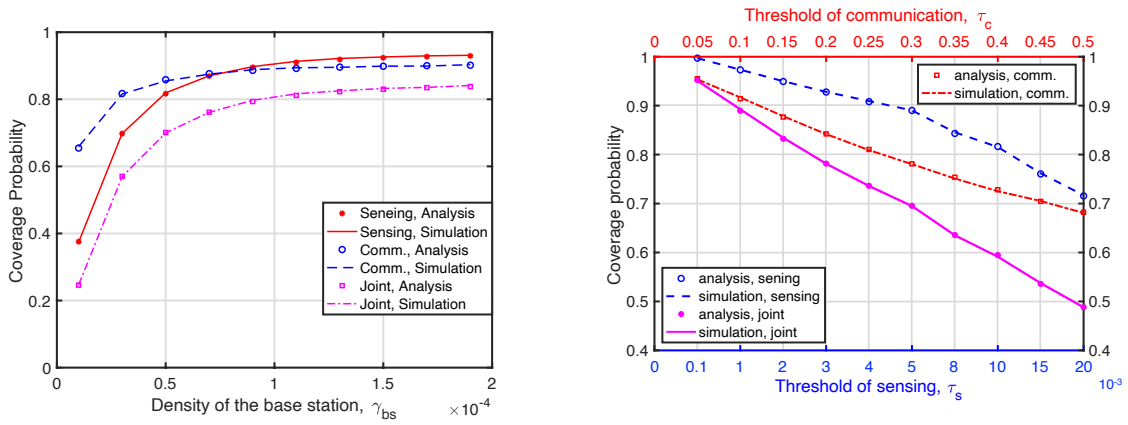

(a) xxx (b) xxx

Fig. 7: Comparison of the analysis and the simulation results

abcd abcd abcd abcd abcd abcd abcd abcd

REFERENCES

[1] J. A. Zhang, M. L. Rahman, K. Wu, X. Huang, Y. J. Guo, S. Chen, and J. Yuan, "Enabling joint communication and radar sensing in mobile networks – a survey," no. arXiv:2006.07559, Oct 2021, arXiv:2006.07559 [cs, eess]. [Online]. Available: http://arxiv.org/abs/2006.07559

[2] N. R. Olson, J. G. Andrews, and R. W. Heath Jr, "Coverage and capacity of joint communication and sensing in wireless networks," no. arXiv:2210.02289, Oct 2022, arXiv:2210.02289 [cs, math]. [Online]. Available: http://arxiv.org/abs/2210.02289

[3] K. S. Ali and M. Chafii, "Integrated sensing and communication for large networks using a dynamic transmission strategy and full duplex," no. arXiv:2211.09466, Nov 2022, arXiv:2211.09466 [cs, eess, math]. [Online]. Available: http://arxiv.org/abs/2211.09466

[4] S. S. Ram and G. Ghatak, "Optimization of network throughput of joint radar communication system using stochastic geometry," no. arXiv:2201.03221, Jan 2022, arXiv:2201.03221 [eess]. [Online]. Available: http://arxiv.org/abs/2201.03221

[5] Z. Fang, Z. Wei, Z. Feng, X. Chen, and Z. Guo, "Performance of joint radar and communication enabled cooperative detection," in *2019 IEEE/CIC International Conference on Communications in China (ICCC)*, Aug 2019, p. 753758.

[6] D. Ghozlani, A. Omri, S. Bouallegue, H. Chamkhia, and R. Bouallegue, "Stochastic geometry-based analysis of joint radar and communication-enabled cooperative detection systems," in *2021 17th International Conference on Wireless and Mobile Computing, Networking and Communications (WiMob)*, Oct 2021, p. 325330.

[7] P. Ren, A. Munari, and M. Petrova, "Performance tradeoffs of joint radar-communication networks," *IEEE Wireless Communications Letters*, vol. 8, no. 1, pp. 165–168, 2019.

[8] F. D. S. Moulin, C. Wiame, L. Vandendorpe, and C. Oestges, "Joint performance metrics for integrated sensing and communication systems in automotive scenarios," no. arXiv:2208.12790, Aug 2022. [Online]. Available: http://arxiv.org/abs/2208.12790

[9] M. I. Skolnik, *Radar handbook*. McGraw-Hill Education, 2008.

[10] "P.1411-10: propagation data and prediction methods for the planning of short-range outdoor radiocommunication systems and radio local area networks in the frequency range 300 MHz to 100 GHz," available at https://www.itu.int/rec/R-REC-P.1411/en, accessed Nov. 20, 2021.

[11] "P.676-13: attenuation by atmospheric gases and related effects," available at https://www.itu.int/rec/R-REC-P.676, accessed Nov. 20, 2021.

[12] "P.530-18: propagation data and prediction methods required for the design of terrestrial line-of-sight systems," available at https://www.itu.int/rec/R-REC-P.530-18-202109-I/en, accessed Nov. 20, 2021.

[13] L. Ippolito, "Radio propagation for space communications systems," *Proceedings of the IEEE*, vol. 69, no. 6, p. 697727, Jun 1981.

[14] Y. Niu, Y. Li, D. Jin, L. Su, and A. V. Vasilakos, "A survey of millimeter wave (mmwave) communications for 5g: Opportunities and challenges," no. arXiv:1502.07228, Feb 2015, arXiv:1502.07228 [cs]. [Online]. Available: http://arxiv.org/abs/1502.07228

[15] T. S. Rappaport, S. Sun, R. Mayzus, H. Zhao, Y. Azar, K. Wang, G. N. Wong, J. K. Schulz, M. Samimi, and F. Gutierrez, "Millimeter wave mobile communications for 5g cellular: It will work!" *IEEE Access*, vol. 1, p. 335349, 2013.

[16] S. Kutty and D. Sen, "Beamforming for millimeter wave communications: An inclusive survey," *IEEE Communications Surveys & Tutorials*, vol. 18, no. 2, p. 949973, 2016.

[17] "IEEE standard for radar definitions," *IEEE Std 686-2017 (Revision of IEEE Std 686-2008)*, Sept. 2017.

[18] J. G. Andrews, A. K. Gupta, and H. S. Dhillon, "A primer on cellular network analysis using stochastic geometry," *arXiv:1604.03183 [cs, math]*, Oct 2016, arXiv: 1604.03183. [Online]. Available: http://arxiv.org/abs/1604.03183

[19] J. Xu, M. A. Kishk, and M.-S. Alouini, "Coverage enhancement of underwater internet of things using multilevel acoustic communication networks," *IEEE Internet of Things Journal*, vol. 9, no. 24, pp. 25 373–25 385, 2022.

[20] H. Kobayashi, B. L. Mark, and W. Turin, *Probability, Random Processes, and Statistical Analysis*. Cambridge: Cambridge University Press, 2011. [Online]. Available: http://ebooks.cambridge.org/ref/id/CBO9780511977770

[21] "AWR2944 single-chip 76- and 81-Ghz FMCW radar sensor datasheet." Available at https://www.ti.com/product/AWR2944, accessed Mar. 20, 2023.

[22] X. Wang, L. Kong, F. Kong, F. Qiu, M. Xia, S. Arnon, and G. Chen, "Millimeter wave communication: A comprehensive survey," *IEEE Communications Surveys & Tutorials*, vol. 20, no. 3, pp. 1616–1653, 2018.